RSC Advances

PAPER

View Article Online
View Journal | View Issue

Check for updates

Cite this: *RSC Adv.*, 2021, **11**, 37120

Tunable formaldehyde sensing properties of palladium cluster decorated graphene†

Lunwei Yang,[abcd] Wei Xiao,[abc] Jianwei Wang,[abc] Xiaowu Li[d] and Ligen Wang*[abc]

The ability to tune the adsorption strength of the targeted gas on sensing materials is crucial for sensing applications. By employing first-principles calculations the adsorption and sensing properties of HCHO on small Pd_n (n = 1–6) cluster decorated graphene have been systematically investigated. The adsorption energy is found to depend on the size of the Pd_n cluster and can be tuned in a wide range from −0.68 eV on Pd(111) to −1.98 eV on the Pd_3/graphene system. We also find that the Pd_n/graphene (n = 5 and 6) systems have an appropriate adsorption energy for HCHO gas sensing. The current–voltage curves are calculated by the non-equilibrium Green's function method for the two-probe nano-sensor devices along both the armchair and zigzag directions. The devices constructed with Pd_n/graphene (n = 5 and 6), having the highest absolute response over 20% at small voltages, should be applicable for HCHO detection. This work provides a theoretical basis for exploring potential applications of metal cluster decorated graphene for gas sensing.

Received 16th September 2021
Accepted 12th November 2021

DOI: 10.1039/d1ra06940c

rsc.li/rsc-advances

Open Access Article. Published on 18 November 2021. Downloaded on 12/4/2025 3:34:31 PM.
This article is licensed under a Creative Commons Attribution-NonCommercial 3.0 Unported Licence.

1. Introduction

Formaldehyde is one of the volatile organic compounds (VOCs) that is chronically and slowly emitted and evaporated from upholstery, carpeting, adhesives, wood and plate products, furniture, and lacquer which are widely used in house construction and decoration.[1,2] Moreover, it is an essential ingredient of consumer goods, such as shampoos, soap, and detergents, and utilized in pharmacology and medicine because of its disinfection effect. Exposure in the circumstances of formaldehyde has been confirmed as a crucial cause of sick building syndrome (SBS) to humans and animals.[2,3] The most common health detriment from formaldehyde is an irritation of the eyes, nose, throat, and skin mucous membrane, and with the increase in the formaldehyde concentration, nausea, cough, headache and other symptoms can appear. Under conditions of unusually high or prolonged exposure, formaldehyde is categorized as a mutagen and possible human carcinogen and teratogens.[4–6] Therefore, efficient and convenient methods to detect formaldehyde have been strongly demanded for indoor and outdoor environmental measurement and control. The development of formaldehyde sensors is thought to be a desirable means for the gas monitoring because the gas sensors own the advantages of excellent selectivity, fast response, low time-consumption, simple operation, and real-time detection *in situ* condition.[7–9]

The graphene decorated by metal nanostructures has become promising materials for various applications, such as chemical sensors, electronic devices, energy storage and fuel cells.[10,11] These materials have caught great scientific and technological interests.[12–15] Recently, the graphene sheets functionalized with metal nanoparticles had shown to increase the selectivity, sensitivity, limit of detection, response, or an unio of these performances.[16–19] Gutés *et al.*[16] exploited an simple and easy-to-implement method of electroless deposition of Au nanoparticles to fabricate Au-decorated graphene sensor for H_2S detecting in relatively fast response. Dong *et al.*[17] developed a biosensor synthesized by assembling Au–Pd/graphene nanocomposites with high electroactive surface and electrical conductivity, which resulted in sensing toward H_2O_2 in cancer cell with a low detection limit, a good linear range, and a rapid response. Kumar *et al.*[18] reported the fast response and recovery of H_2 sensing of Pd–Pt alloy nanoparticle-graphene composite layers fabricated using chemical methods. Fan *et al.*[19] found that Au nanoparticles decorated graphene could enhanced the NO_2 detecting with fast response, good reversibility and mechanical stability, and high sensitivity. It had demonstrated that palladium nanoparticles could be the very effective oxidation catalysts and electrochemical sensors for formaldehyde.[12,13,20–23] The formaldehyde detecting properties of single-walled carbon nanotube hybridized with Pd were investigated by density-functional theory calculations.[22] These researches indicated that metal nanoparticles decorated

[a]*State Key Laboratory of Nonferrous Metals and Processes, GRINM Group Co., Ltd., Beijing 100088, P. R. China. E-mail: lg_wang1@yahoo.com*
[b]*GRIMAT Engineering Institute Co., Ltd., Beijing 101407, P. R. China*
[c]*General Research Institute for Nonferrous Metals, Beijing 100088, P. R. China*
[d]*Department of Materials Physics and Chemistry, School of Materials Science and Engineering, Key Laboratory for Anisotropy and Texture of Materials, Ministry of Education, Northeastern University, Shenyang, 110819, P. R. China*

† Electronic supplementary information (ESI) available. See DOI: 10.1039/d1ra06940c

© 2021 The Author(s). Published by the Royal Society of Chemistry

Open Access Article. Published on 18 November 2021. Downloaded on 12/4/2025 3:34:31 PM.
This article is licensed under a Creative Commons Attribution-NonCommercial 3.0 Unported Licence.

graphene shows a great potential for applying to the gas sensing and catalysis.

In this paper, we investigate the HCHO absorption and sensing properties of Pd_n ($n = 1$–6) clusters supported on graphene by using non-equilibrium Green's function (NEGF) method combined with the density-functional theory (DFT). We find that it is possible to adjust the adsorption strength of HCHO gas on Pd_n ($n = 1$–6) clusters supported on graphene by changing the size of Pd_n cluster. As increasing the size of Pd cluster the adsorption strength decreases and the adsorption energy approaches the value of -0.68 eV for the HCHO adsorption on Pd(111), which is beyond the low limit of targeted gas adsorption energy -0.8 eV required by good sensitivity.[24] The geometries of Pd_n nanoclusters supported on graphene for the both cases with and without HCHO adsorption are optimized, and the HCHO adsorption energies are calculated. The two-probe nano-sensor devices consisted of the left/right electrodes and the central scattering region are constructed, and the current–voltage curves and sensor responses are simulated. The results indicate that the systems of Pd_n ($n = 5$ and 6) clusters supported on graphene having the proper adsorption energy and a large enough response at low bias voltages are promising for HCHO sensing applications.

2. Computational details

All the structural optimizations and electronic property calculations are performed by using the Vienna *Ab initio* Simulation Package (VASP),[25,26] adopting the generalized gradient approximation (GGA) in the Perdew, Burke and Ernzernhof (PBE) functional[27] for exchange-correlation potential and the projector augmented wave (PAW) method[28] to describe the electron–ion interaction. A conjugate-gradient (CG) algorithm is performed to relax all the ions until the force acting on each ion is less than 0.01 eV $Å^{-1}$. The graphene is modelled by a (4×4) supercell containing 32 carbon atoms and a 15 Å thick vacuum in the z direction which is perpendicular to the graphene surface. A large (5×5) supercell is also used for testing the lateral interaction imposed by the periodic boundary conditions and we find that the lateral interaction in the (4×4) graphene supercell model is negligible. The vacuum thickness is large enough to avoid interactions with the adjacent cells due to the periodic boundary conditions enforced in the calculations. The following electronic states are chosen as the valence electron configurations in the pseudopotential description of the system: 1s for H, 2s2p for C and O, and 4d5s for Pd. A semi-empirical DFT-D2 (ref. 29) correction is employed to describe van der Waals interactions between the graphene substrate and gas molecule. The more sophisticated D3 correction method has also tested in our calculations and the results show that the HCHO adsorptions on Pd_n/graphene become slightly weaker by about 0.1 eV. The plane-wave cutoff energy is set to be 500 eV, and a Gaussian smearing for the occupation of the electronic levels has been adopted in all DFT simulations. The Brillouin zone integrations are performed with $5 \times 5 \times 1$ and $15 \times 15 \times 1$ Monkhorst–Pack meshes for atomic relaxations and electronic structure calculations, respectively. The theoretical C–C bond length in graphene is 1.43 Å, which is in excellent agreement with the previous work.[30] For HCHO adsorption on the Pd_n/graphene substrate, the charge transfer Δq is obtained based on the Bader charge analysis.[31,32] Positive Δq means the electron gain of adsorbed gas molecule from the substrate.

The formaldehyde adsorption energy on the Pd_n/graphene substrate is calculated as follows:

$$E_{ads} = E_{HCHO\text{–}Pd_n/Gr} - E_{Pd_n/Gr} - E_{HCHO} \quad (1)$$

where $E_{HCHO\text{–}Pd_n/Gr}$, $E_{Pd_n/Gr}$ and E_{HCHO} represent the total energies of the system of HCHO molecule adsorbed on Pd_n/graphene substrate, the Pd_n cluster loaded on graphene substrate and an isolated HCHO molecule, respectively. A negative E_{ads} means that the adsorption is exothermic.

The electronic transport properties are investigated by Nanodcal,[33,34] which employs the non-equilibrium Green's function technique with the Keldysh formalism in combination with DFT.[35,36] The GGA-PBE functional[27] is adopted as the exchange-correlation potential and double ζ-plus basis (DZP) is employed for the basis set. The real space mesh cutoff energy is 100 Ha, and the Brillouin zone samplings are represented by Monkhorst–Pack mesh of $1 \times 15 \times 1$ and $1 \times 15 \times 100$ k-points for the electrode and central region of the two-probe geometry, respectively.

The electronic transmission function through the device is obtained by the Landauer formula,[37] as follows

$$T(E,V_b) = T_r[\Gamma_L(E)G^R(E)\Gamma_R(E)G^A(E)] \quad (2)$$

where $G^{R/A}$ is the retarded/advanced Green's function in the central scattering region, and $\Gamma_{L/R}$ is the coupling matrix between the central zone and the left/right leads.[33] The transmission around the Fermi energy at the equilibrium state is $T(E,V) = T_r[\Gamma_L G^R \Gamma_R G^A]$, which represents the probability that an electron with the energy E transmits from the left electrode into the right one. For non-equilibrium transport properties, the electrochemical potentials $\mu_{L/R} = \mu \pm eV_b/2$, where μ and V_b are the Fermi level and the applied bias, are applied to the left and right electrodes, respectively. The current through the device is given using the Landauer–Büttiker equation,[38]

$$I(V_b) = G_0 \int T(E,V_b)[f(E-\mu_L) - f(E-\mu_R)]dE \quad (3)$$

where the $G_0 = \frac{2e}{h}$ is the unit of the quantum conductance and $f(E-\mu_{L/R})$ is the Fermi–Dirac distribution function of the left/right electrode.

3. Results and discussion

3.1 Geometries of free-standing and graphene-supported Pd_n clusters

The free-standing Pd_n clusters with 2–6 atoms are relaxed and the optimized structures are displayed in Fig. 1. As shown in Fig. 1, the average Pd–Pd bond length of a Pd_n cluster increases with increasing its cluster size and gradually approaches to the bond length of 2.75 Å for the Pd bulk phase. The bond length

Open Access Article. Published on 18 November 2021. Downloaded on 12/4/2025 3:34:31 PM.
This article is licensed under a Creative Commons Attribution-NonCommercial 3.0 Unported Licence.

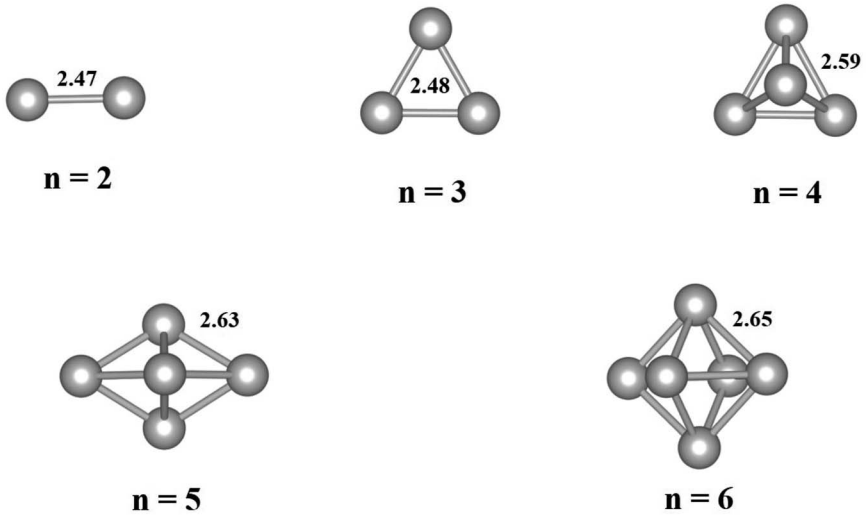

Fig. 1 Optimized geometries of free-standing Pd_n ($n = 2$–6) clusters. The average Pd–Pd bond lengths (in Å) are given for the clusters. Gray balls represent Pd atoms.

results are in good agreement with those values in literature.[39] For the Pd_n ($n \geq 4$) clusters the three-dimensional (3D) structure is energetically more favorable than the flat one.

There are multiple ways to build a Pd_n cluster loaded on the graphene substrate. We have employed two different approaches to search for the most stable atomic configuration of a Pd_n cluster loaded on graphene. In the first approach, the optimized Pd_n clusters as shown in Fig. 1 are placed on the graphene surface in various orientations, and in the second approach the Pd_n/graphene structure is built by adding Pd atoms one by one to previously optimized Pd_{n-1}/graphene at some possible positions. After relaxing all the atomic configurations, the most stable structures of Pd_n/graphene are shown in Fig. 2 and the structural files are also provided as ESI.† Their structural and energetic results are presented in Table 1. In Table 1, d_{Pd-Pd} and $d_{Pd-C(Gr)}$ are the average Pd–Pd bond length in the Pd_n clusters and the shortest distance between the Pd atom and the C atom of graphene, respectively. A single Pd atom on the graphene surface prefers to occupy the bridge site as shown in Fig. 2(a). Similar to the single Pd atom case, for the Pd_n ($n = 2$ & 3) clusters all Pd atoms prefer to occupy the bridge sites. For a larger Pd_n ($n = 4$–6) cluster it tends to have a 3D

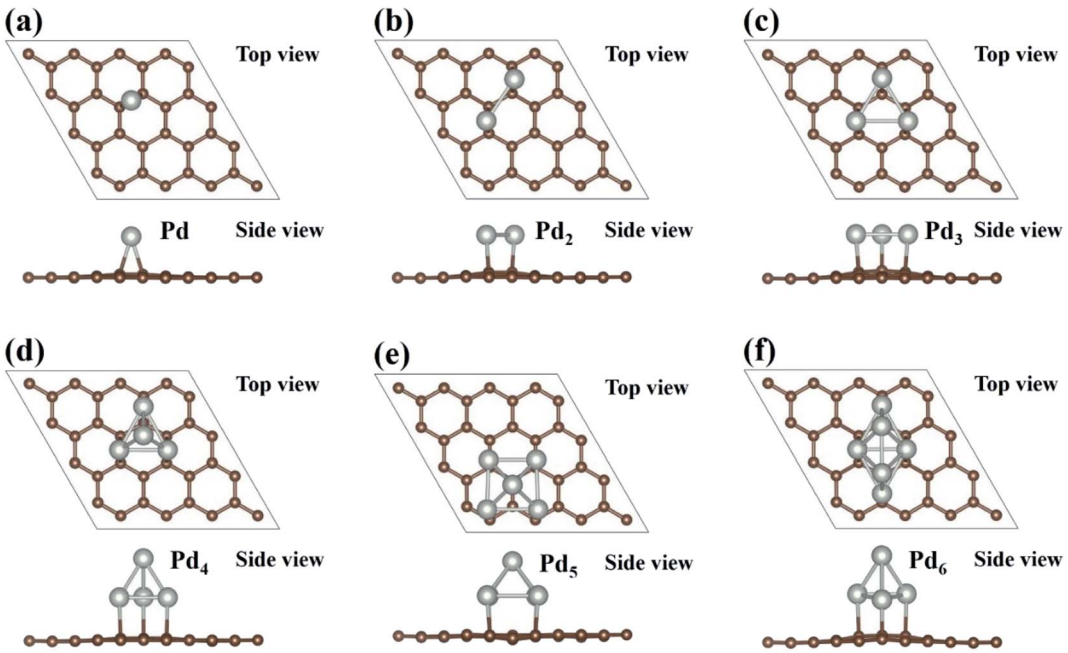

Fig. 2 The most stable configurations of Pd_n ($n = 1$–6) clusters supported on graphene are presented in (a–f). Brown and sliver balls represent the C and Pd atoms, respectively.

© 2021 The Author(s). Published by the Royal Society of Chemistry

Open Access Article. Published on 18 November 2021. Downloaded on 12/4/2025 3:34:31 PM.
This article is licensed under a Creative Commons Attribution-NonCommercial 3.0 Unported Licence.

Table 1 Optimized geometric and energetic results of Pd_n ($n = 1$–6) clusters supported on graphene. The average Pd–Pd bond length d_{Pd-Pd} in Pd_n clusters and the average Pd–C bond length $d_{Pd-C(Gr)}$ between Pd atom and adjacent C atom in graphene are also presented in the table

Clusters	d_{Pd-Pd} (Å)	$d_{Pd-C(Gr)}$ (Å)	E_b (eV)	E_{int} (eV)
Pd_1	—	2.18	−1.10	−1.10
Pd_2	2.71	2.20	−1.35	−1.44
Pd_3	2.75	2.22	−1.52	−0.79
Pd_4	2.63	2.34	−1.85	−0.67
Pd_5	2.66	2.41	−1.94	−0.66
Pd_6	2.74	2.28	−2.07	−0.66

structure. The supported Pd_5 and Pd_6 clusters have very different atomic configurations from those free-standing ones, while the supported Pd_n ($n = 2$–4) clusters have the same shape as the free-standing ones although their average Pd–Pd bond lengths are enlarged. The Pd_n ($n = 4$–6) clusters have the shapes of tetrahedron, hexahedron and octahedron, respectively.[39] The Pd–Pd bond lengths in the Pd_n clusters on the graphene surface vary in an irregular way and appear to oscillate as shown in Table 1, which is a general phenomenon well known for isolated metal clusters.[40] The distances $d_{Pd-C(Gr)}$ between the Pd atom and the C atom of graphene are also larger for the large Pd_n ($n =$ 4–6) clusters compared to those for the small Pd_n ($n = 1$–3) clusters, as shown in Table 1. This may be associated with the 2D–3D structure transformation of Pd_n clusters. Overall, our final stable Pd_n structures supported on the graphene substrate are very close to those obtained in ref. 39 and 40.

To evaluate the stability of a Pd_n cluster loaded on graphene, the binding energy E_b is calculated as follows

$$E_b = [E_{Pd_n/Gr} - n \times E_{Pd} - E_{Gr}]/n \quad (4)$$

where $E_{Pd_n/Gr}$ is same as it in eqn (1), E_{Gr} and E_{Pd} are the energies of the graphene supercell and free Pd atom, respectively. The interaction energy between the Pd_n cluster and graphene is defined as

$$E_{int} = E_{Pd_n/Gr} - E_{Pd_n} - E_{Gr} \quad (5)$$

where E_{Pd_n} is the energy of the free-standing Pd_n cluster, and the others on the right side of the equation are same as those in eqn (4). The interaction energy E_{int} is to evaluate the interaction between the Pd_n cluster and the graphene substrate, while the binding energy E_b represents the stability of the system, *i.e.* the average formation energy per Pd atom.

We plot E_b and E_{int} as a function of the Pd_n cluster size in Fig. 3. The binding energy is almost linearly dependent on the Pd cluster size. With increasing the cluster size, the cluster becomes more stable. The stability increase of the Pd_n cluster supported on graphene is mainly attributed to the formation of Pd–Pd bonds. For example, for the Pd_2 cluster the binding energy (per Pd atom) is 0.25 eV lower than that of Pd_1 supported on graphene, which can be caused by the Pd–Pd bond formed in the cluster. For the interaction energy E_{int} in Fig. 3(b), it shows that the interaction between the Pd_n cluster and graphene is stronger for the small Pd_n ($n = 1$–3) cases relative to the large Pd_n ($n = 4$–6) cases. The moderate interaction of about −0.66 eV for the large Pd_n ($n = 4$–6) cases may explain their atomic structure changes and electron scattering effects upon HCHO adsorption, as discussed below. The interaction energy results are in agreement with the previous studies by Cabria *et al.*[41] and Xiao *et al.*[42]

3.2 Formaldehyde adsorption on Pd(111) and Pd_n/graphene

The formaldehyde adsorption on the Pd(111) surface is calculated, and the adsorption energy is defined as $E_{ads}^{Pd(111)} = E_{HCHO-Pd(111)} - E_{Pd(111)} - E_{HCHO}$. $E_{HCHO-Pd(111)}$ is the total energy of a formaldehyde molecule adsorbed on the Pd(111) slab, and $E_{Pd(111)}$ and E_{HCHO} are the total energies of the Pd(111) slab and the isolated formaldehyde molecule, respectively. The slab model consisting of five Pd atomic layers and a vacuum thickness of 15 Å is constructed with the theoretical equilibrium lattice constant of 3.89 Å and a (3×3) surface supercell. The adsorbed HCHO and Pd atoms in the top three layers are allowed to relax, while the atoms in the bottom two layers are fixed at the bulk lattice sites. After full structure relaxation, the most stable absorption geometry is obtained, in which the carbonyl group of HCHO gas molecule is parallel to the Pd(111) surface and both the C and O atoms bond to Pd atoms with the bond lengths of 2.17 Å and 2.14 Å, respectively. The calculated adsorption energy E_{ads} is −0.68 eV, which is at least 0.25 eV lower than those for different adsorption geometries, such as the one that only O atom is formed the bond with the Pd atom on the surface. The result is in good agreement with previous works.[23,43,44]

The adsorptions of HCHO molecule on the Pd_n ($n = 1$–6) clusters supported on graphene have been investigated. The initial HCHO adsorption geometries are built by considering various possible orientations of the HCHO molecule and adsorption sites. We fully relax the initial HCHO adsorption structures and obtain the most stable adsorption atomic configuration for each case. The optimized atomic configurations and the corresponding adsorption energies are presented in Fig. 4 and Table 2. In Fig. 4, we can see that the adsorbed HCHO molecule is bonded to the Pd_n clusters supported on graphene through both C and O atoms of HCHO molecule, which is similar to the HCHO adsorption on Pd(111).[43] Moreover, the interaction of adsorbed HCHO molecule with the Pd_n cluster can dramatically affect the atomic configurations of the Pd_n clusters supported on graphene. For example, for the Pd_1 case the Pd atom at the bridge site on graphene has been moved to the atop site upon HCHO adsorption, and the Pd atom in the top atomic layer of the Pd_4 cluster moves away from the vertex site to the bridge site between two Pd atoms. For the Pd_5 cluster the square base has been changed to the parallelogram shape, while for the Pd_6 cluster two Pd atoms in the top atomic layer move to the bridge sites from the hollow sites upon HCHO adsorption. However, we hope that the Pd_n clusters can resume their original atomic configurations in Fig. 2 after HCHO desorption and are applicable to HCHO detecting.

Open Access Article. Published on 18 November 2021. Downloaded on 12/4/2025 3:34:31 PM.
This article is licensed under a Creative Commons Attribution-NonCommercial 3.0 Unported Licence.

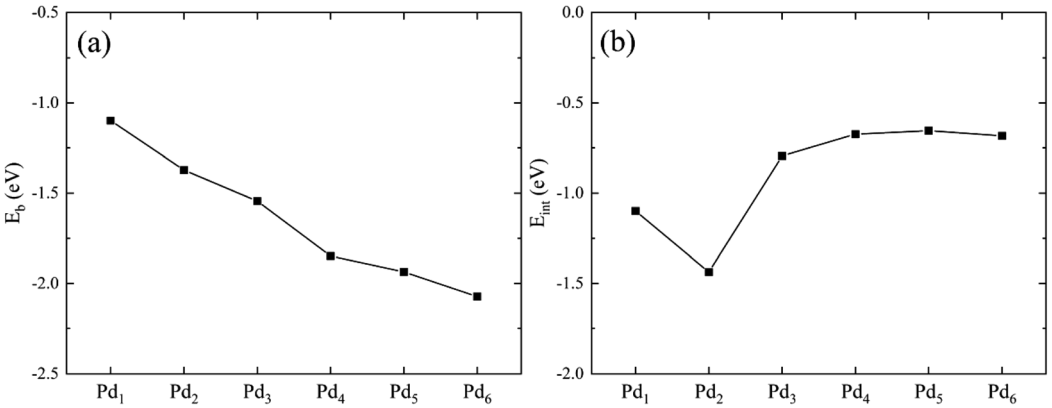

Fig. 3 The binding energy E_b (a) and the interaction energy E_{int} between the Pd_n cluster and the graphene substrate (b) as a function of the cluster size.

Table 2 Optimized atomic structures and adsorption energies of HCHO molecule absorbed on Pd_n/graphene and Pd(111). The d_{C-O} is the C–O bond length in the adsorbed HCHO molecule. The electron gains of the adsorbed HCHO molecule Δq_{HCHO} and graphene without HCHO adsorption Δq_{Grap} and with HCHO adsorption Δq_{Grap} (HCHO) are obtained by the Bader charge analysis, and the HCHO adsorption energies E_{ads} are calculated according to eqn (1)

Clusters	d_{C-O} (Å)	Δq_{HCHO}	Δq_{Grap}	Δq_{Grap} (HCHO)	E_{ads} (eV)
Pd_1	1.29	0.25	0.17	0.08	−1.42
Pd_2	1.32	0.36	0.24	0.19	−1.83
Pd_3	1.34	0.39	0.31	0.33	−1.98
Pd_4	1.33	0.36	0.26	0.29	−1.49
Pd_5	1.32	0.34	0.30	0.32	−1.17
Pd_6	1.31	0.32	0.30	0.31	−1.03
$Pd_{(111)}$	1.32	0.26	—	—	−0.68

The HCHO adsorption energies on the Pd_n clusters supported on graphene are plotted in Fig. 5. The HCHO adsorption becomes stronger from Pd_1 to Pd_3 clusters, and then becomes weaker when further increasing the size of the Pd_n cluster. The strongest adsorption for the Pd_3 cluster supported on graphene has the adsorption energy of −1.98 eV. The adsorption on the 3D Pd_n clusters is weaker compared to those on the 2D Pd_n clusters, and it gradually approaches the adsorption energy of −0.68 eV on Pd(111) as the size of Pd_n cluster increases. This large adsorption energy difference of 1.30 eV between the adsorptions on the Pd_3 cluster and Pd(111) makes it feasible to tune the HCHO adsorption strength on the Pd_n cluster decorated graphene by adjusting its size. The adsorption strength on the Pd_n ($n = 5$ and 6) cluster decorated graphene is in the proper adsorption energy range, implying their potential applications as HCHO sensors. The adsorption strength between the targeted gas and sensing materials is a key factor for sensor applications because it needs to balance the sensitivity and the recovery time. In a previous work,[45] the authors investigated HCHO adsorption on Ti- and V-doped graphene and estimated the recovery times to be 10^{-3} s and 10^4 s corresponding to the adsorption energies of −1.12 eV and −1.94 eV, respectively. Therefore, in our previous work[24] we suggested that the adsorption energy should be in the range of −0.8 to −1.2 eV in order to have a good balance between the sensitivity and the recovery time. From Fig. 5, we also find that there is a certain correlation between the adsorption energy and C–O bond length and charge transfer of HCHO molecule. That is that for the Pd_n cluster system which has a larger C–O bond length and charge transfer, the HCHO adsorption is also stronger, and *vice versa*. For the Pd_3 cluster, for instance, the HCHO adsorption is the strongest while it has the largest C–O bond length and charge transfer.

Compared to the C–O bond length (1.21 Å) of isolated HCHO molecule, the C–O bond of the adsorbed HCHO molecule is enlarged as shown in Table 2 and Fig. 5. The charge transfers of adsorbed HCHO are all positive and it means that the HCHO molecule acts as electron acceptor to gain the electrons from the Pd_n/graphene substrate. We plot the C–O bond length and the charge transfer as a function of the size of Pd_n cluster in Fig. 5(b). As discussed in previous studies[46] the C–O bond length of the adsorbed HCHO molecule on the Pd_n/graphene substrate is closely correlated with its electron gain from the substrate. From Fig. 5, it confirms that there is a similar trend for both the C–O bond length and the electron gain of adsorbed HCHO molecule. With increasing the size of Pd_n cluster, the C–O bond length and the electron gain of HCHO molecule first increase and then decrease. For the Pd_3 cluster case, the C–O bond expands 0.13 Å compared to that of HCHO molecule in the gas phase. The corresponding charge transfer of 0.39*e* is also the largest. A large elongation of the C–O bond implies the bond strength is weakened, which may be caused by the large charge transfer and strong interaction between the molecule and the Pd cluster.

The charge density difference (CDD) is defined as $\Delta\rho = \rho_{HCHO-Pd_n/Gr} - \rho_{HCHO} - \rho_{Pd_n/Gr}$, where $\rho_{HCHO-Pd_n/Gr}$ is the charge density of the interacting system, ρ_{HCHO} and $\rho_{Pd_n/Gr}$ are the charge densities of the isolated HCHO molecule and the Pd_n/graphene substrate, respectively. The 3D iso-surfaces of CDD and the planar-average charge-density difference $\Delta\rho$ along the z axis are plotted in Fig. 6. The cyan and yellow areas of CDD denote the charge depletion and accumulation, respectively,

© 2021 The Author(s). Published by the Royal Society of Chemistry

Open Access Article. Published on 18 November 2021. Downloaded on 12/4/2025 3:34:31 PM.
This article is licensed under a Creative Commons Attribution-NonCommercial 3.0 Unported Licence.

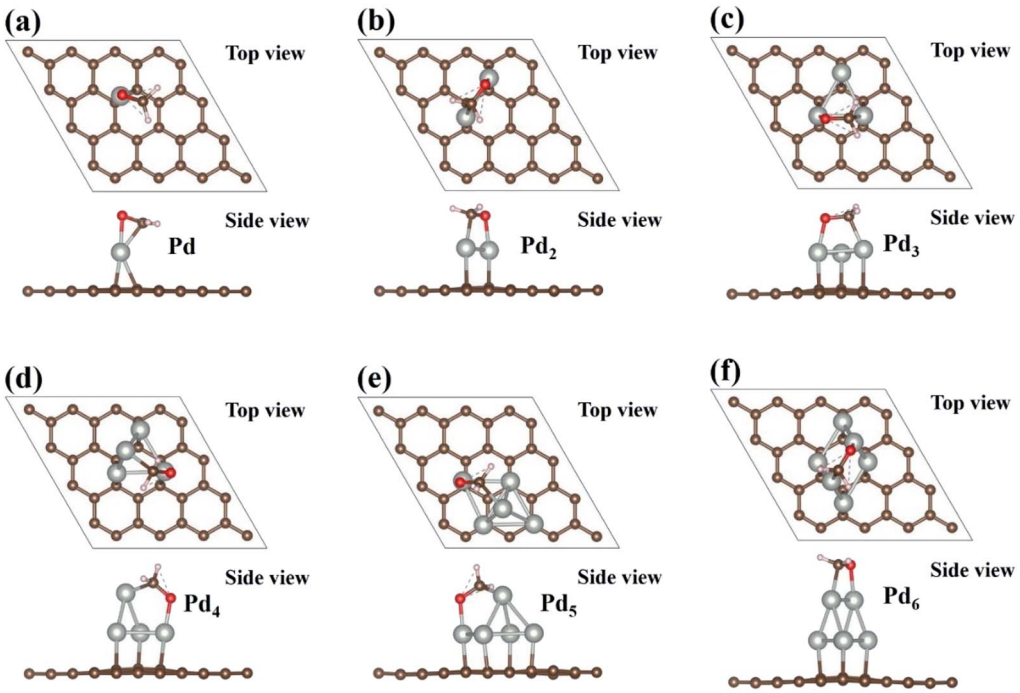

Fig. 4 Optimized geometries of Pd_n ($n = 1–6$) cluster supported on graphene with HCHO adsorption are presented in (a–f). Brown, white, red and sliver balls represent the C, H, O and Pd atoms, respectively.

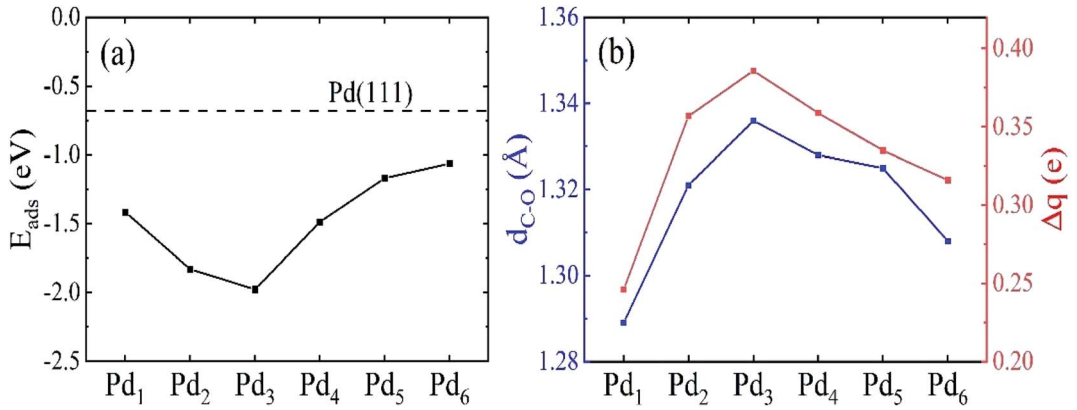

Fig. 5 (a) The HCHO adsorption energy on Pd_n ($n = 1–6$) supported on graphene as a function of the cluster size. The dashed horizontal line in (a) represents the HCHO adsorption energy on Pd(111). (b) The C–O bond length d_{C-O} and charge transfer Δq of the adsorbed HCHO molecule on Pd_n/graphene.

and the iso-surface level is set to 0.002 e $Å^{-3}$. Positive values of the planar-average $\Delta\rho$ indicate the electron gain at the z-axis transverse section. The adsorption of HCHO molecule onto Pd_n/graphene can greatly change the charge distribution. Obviously, there is an electron accumulation between the O or C atom of HCHO and the Pd atom that it is bonded to. From the planar-average $\Delta\rho$ for the Pd_2 and Pd_3 cases, it can clearly see that the largest electron gain is located the middle region of the C–Pd and O–Pd bonds. The CCD results in Fig. 6 verify that the HCHO molecule gains electrons from the substrate, which is consistent with the Bader charge analyses.

3.3 Formaldehyde sensing properties of Pd_n/graphene

The HCHO sensing properties of the Pd_n/graphene systems are carried out by the NEGF-DFT method.[47,48] Because of the anisotropy of graphene lattice, the nano-sensor devices are modeled for two different transport directions, *i.e.* the armchair- and zigzag-directions. The two-probe devices are consisted of the left/right electrode, the central scattering region that is made up with the Pd_n cluster supported on the graphene with/without HCHO adsorption. For the Pd_n clusters on graphene without and with HCHO gas adsorption the optimized atomic structures are presented in Fig. 2 and 4, and these

Open Access Article. Published on 18 November 2021. Downloaded on 12/4/2025 3:34:31 PM.
This article is licensed under a Creative Commons Attribution-NonCommercial 3.0 Unported Licence.

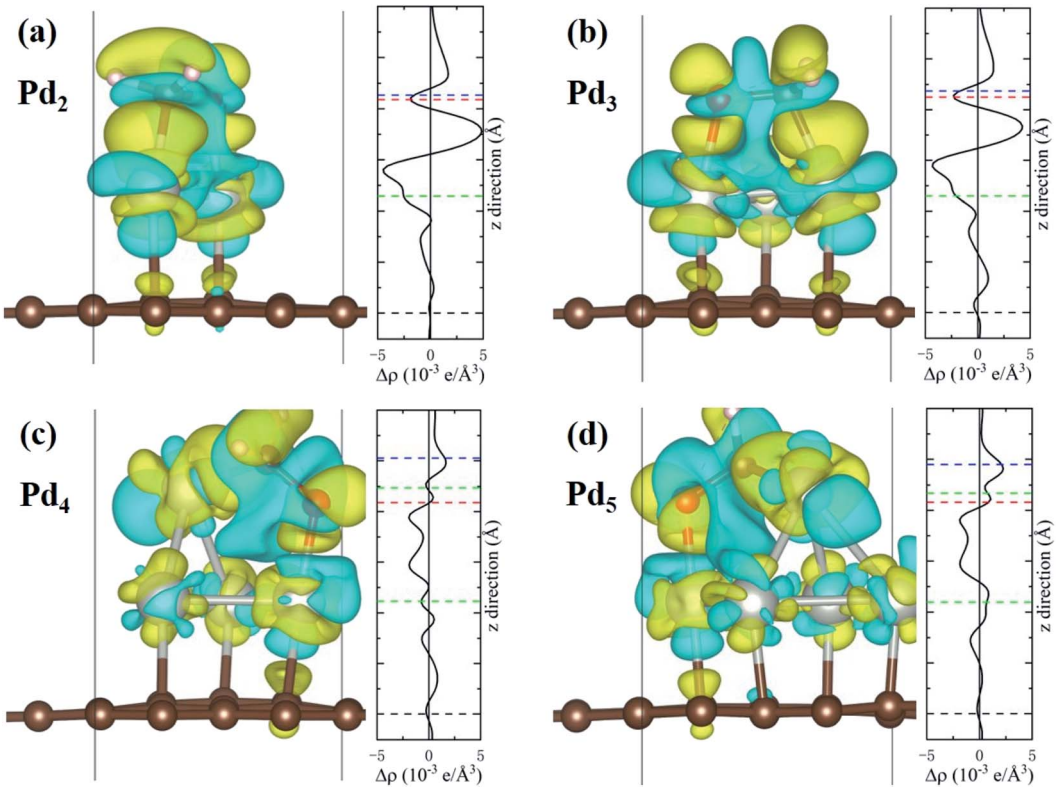

Fig. 6 The charge density differences for the HCHO molecule adsorbed on Pd_n/graphene ($n = 2$–5) together with the planar-average charge-density $\Delta\rho$ along the z axis are shown in (a–d). The iso-surface corresponds to the value of 0.002 e Å^{-3}. The yellow and cyan regions represent charge accumulation and depletion, respectively. The dashed black, green, blue and red lines in the planar-average $\Delta\rho$ mark the average positions of the graphene plane, Pd, C and O atoms of HCHO molecule in the z coordinates. The two dashed green lines in (c) and (d) refer to the two different Pd atomic layers.

stable structures do not need to optimize again since they are independent of the transport directions. The sensor models, using HCHO adsorption on Pd_3/graphene as the example, are illustrated in Fig. 7. The atomic structures of the central scattering region are fully relaxed as discussed above.

The sensing performance can be evaluated in terms of the sensor response (S),[49,50] which is defined as the resistance difference after gas adsorption and before gas adsorption divided by the resistance without gas adsorption. According to this definition, we have $S = [(R_g - R_0)/R_0] \times 100\% = [(I_0 - I_g)/I_g] \times 100\%$, in which the initial electronic resistance/current of the sensor without HCHO adsorption is R_0/I_0 and the resistance/current with HCHO adsorption is R_g/I_g. We have simulated the current–voltage (I–V) curves of all the Pd_n/graphene cases with and without HCHO adsorption under the bias voltage from 0 to 1 V. The I–V and response results are presented in Fig. 8.

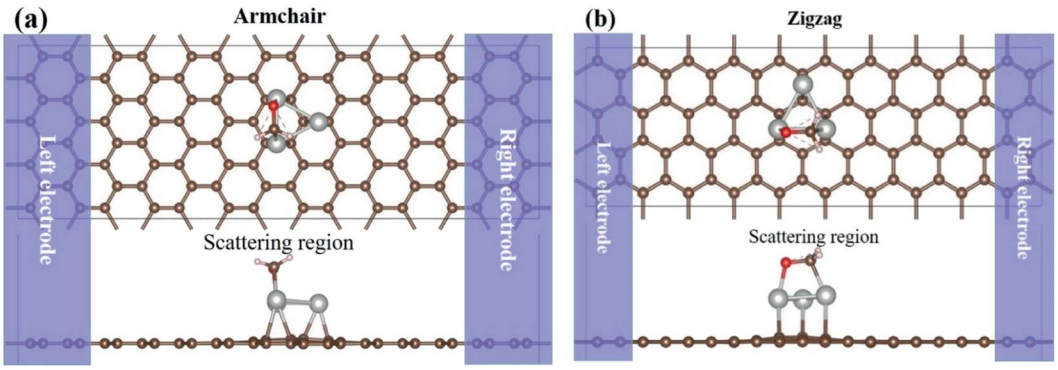

Fig. 7 Two-probe nano-sensor device models, using HCHO adsorption on Pd_3/graphene as the example. The semi-infinite left and right graphene electrodes (shaded zones) are in contact with the scattering region. Both the top and side views of the devices along the armchair (a) and zigzag (b) directions are shown. The C, Pd, O and H atoms are shown in brown, silver, red and white balls, respectively.

© 2021 The Author(s). Published by the Royal Society of Chemistry

Open Access Article. Published on 18 November 2021. Downloaded on 12/4/2025 3:34:31 PM.
This article is licensed under a Creative Commons Attribution-NonCommercial 3.0 Unported Licence.

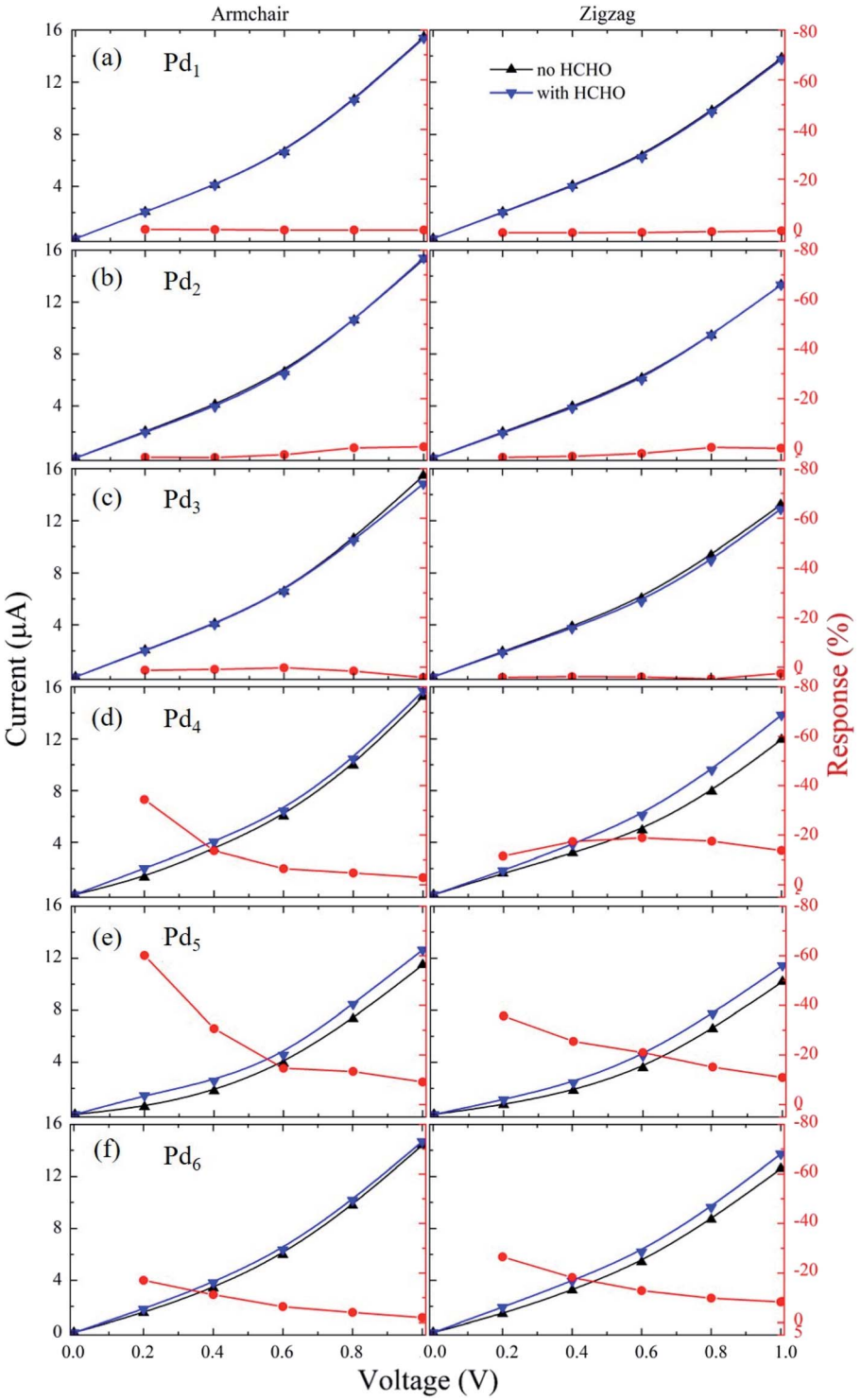

Fig. 8 The current–voltage curves and responses of the armchair- and zigzag-orientated nano-sensor devices constructed from Pd_n/graphene ($n = 1$–6) under the bias voltage from 0 to 1.0 V are presented in (a–f).

The current increases as increasing the applied voltage for all the nano-sensors along both the armchair and zigzag transport directions. For the HCHO molecule adsorption on Pd_n/graphene ($n = 1$–3), it is found that the currents passing through the nano-devices are almost same before and after HCHO adsorption in the whole applied voltage range. So the responses for these nano-sensors are insensitive regarding the HCHO gas adsorption. As shown in Fig. 8(d–f) for the large Pd_n ($n \geq 4$) cluster cases, the electronic current of the sensor with HCHO adsorption starts to differ from that without HCHO adsorption.

© 2021 The Author(s). Published by the Royal Society of Chemistry

Open Access Article. Published on 18 November 2021. Downloaded on 12/4/2025 3:34:31 PM.
This article is licensed under a Creative Commons Attribution-NonCommercial 3.0 Unported Licence.

The current is increased upon the HCHO adsorption relative to the case without HCHO adsorption. The corresponding responses are also substantially larger than those for the Pd_n (n = 1–3) cluster systems. We can see that the sensor response depends on the applied voltage and generally decreases as the applied voltage increases. The dependence of response on the applied voltage will be discussed below. A large response at the small bias voltage implies that the device has a short response time and a high sensitivity. Therefore, these devices with the highest absolute response over 20% at small bias voltages should be sensitive enough for the HCHO gas detecting.[51–53] Especially, for the armchair-orientated Pd_5/graphene nano-sensor it has the highest absolute response over 60% at 0.2 V, indicating its suitability of HCHO sensing.

The transmission spectra in the equilibrium situation with zero bias for the Pd_n/graphene substrate adsorbed with/without HCHO molecule are plotted in Fig. 9. The transmission spectra exhibit a dependence on the size and geometry of the Pd_n cluster. For the Pd_n (n = 1–3) cases, the transmission spectra near zero bias are relatively smoother compared to those for the larger Pd_n (n = 4–6) clusters and almost same before and after HCHO adsorption. This explains why the nano devices consisted of the Pd_n (n = 1–3) clusters are insensitive with respect to the HCHO adsorption for these cases. For the larger Pd_n (n = 4–6) cases we see that the transmission spectra are quite different on the left side of zero bias before and after HCHO adsorption. The transmission spectra vary irregularly without HCHO adsorption, which is mainly attributed to the electron scattering effect of the complex local deformation of graphene loaded with a larger Pd_n cluster. Upon the HCHO adsorption, the interaction between the Pd_n cluster and graphene is weakened caused by the interaction between the HCHO and the Pd_n cluster supported on graphene, and consequently the electron scattering effect of graphene local deformation becomes relatively weaker compared to the case without HCHO adsorption. From Table 2 we can see that for the Pd_n (n = 3–6) cases the graphene electron gains before and after HCHO adsorption have a very small change. The electron gain of graphene for the Pd_3 case is similar to those for other Pd_n (n = 4–6) cases, but the current increases are quite different for all the four cases. This indicates that the current change after HCHO adsorption can be mainly attributed to the graphene scattering effect, rather than the number change of charge carriers. The transmission coefficients for the HCHO adsorption cases are generally larger than those without HCHO adsorption, which is consistent with the current–voltage results in Fig. 8.

In order to understand the larger response under low bias voltages, the transmission spectra of the nano-sensor constructed from Pd_5/graphene along the armchair-direction are presented in Fig. 10. We see that within the voltage window (indicated by the dashed lines) the transmission spectra differ from each other before and after HCHO adsorption. The transmission spectrum change before and after HCHO adsorption results in the response of HCHO adsorption, and the integration of the transmission spectrum within the voltage window determines the current. According to the definition of

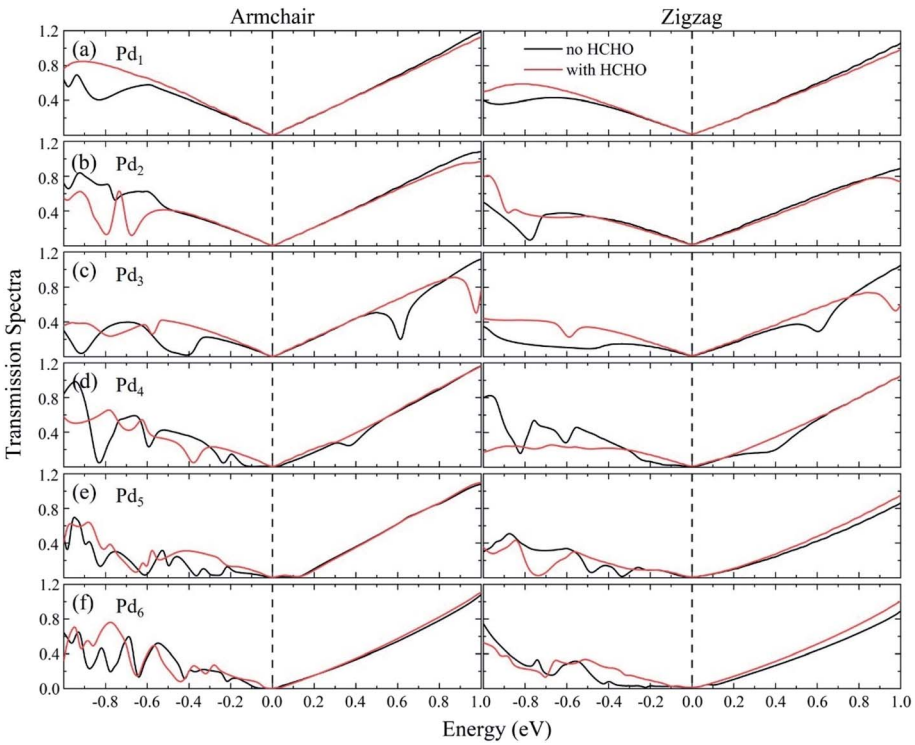

Fig. 9 Transmission spectra for the Pd_n/graphene (n = 1–6) sensors without and with HCHO adsorption at zero bias are shown in (a–f). The dashed lines, which are set to be zero on the energy scale, indicate the Fermi level.

© 2021 The Author(s). Published by the Royal Society of Chemistry

Open Access Article. Published on 18 November 2021. Downloaded on 12/4/2025 3:34:31 PM.
This article is licensed under a Creative Commons Attribution-NonCommercial 3.0 Unported Licence.

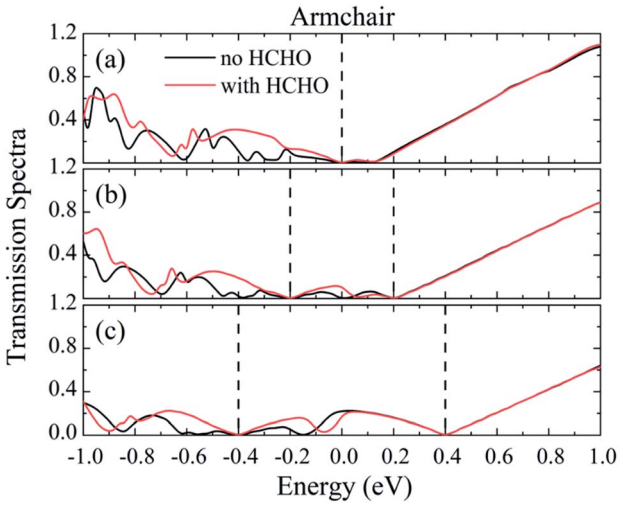

Fig. 10 The transmission spectra of HCHO nano-sensor constructed from Pd_5/graphene along the armchair-direction under (a–c) 0, 0.4 and 0.8 V bias. The dashed lines represent the bias windows.

response, it is the ratio of the current difference before and after gas adsorption to the current without gas adsorption. Since the current is low under low bias voltage the response of nano-sensor under low bias voltages can be larger than those under high bias voltages.

4. Conclusions

The HCHO sensing properties of small Pd_n (n = 1–6) cluster decorated graphene have been systematically investigated by performing first-principles calculations in the framework of density-functional theory. The optimized geometries of Pd_n cluster decorated graphene with and without HCHO adsorption, adsorption energies and charge transfers are obtained and analyzed for various Pd_n cluster cases. The adsorption strength of HCHO gas molecule on the Pd_n cluster decorated graphene is dependent on the cluster size and can be tuned in a wide range from −0.68 eV on Pd(111) to −1.98 eV on the Pd_3 cluster decorated graphene. The calculated results show that the Pd_n (n = 5 and 6) cluster decorated graphene systems have a proper adsorption energy for the HCHO sensing. The adsorbed HCHO gas molecule gains electrons from the Pd_n cluster decorated graphene, acting as an acceptor. The HCHO adsorption strength is found to be correlated with the electron gain and C–O bond length. The two-probe sensor devices consisting of the central scattering region and pristine graphene electrodes with the armchair and zigzag transport directions are built, and the current–voltage curves are calculated by the non-equilibrium Green's function method. The results indicate that the devices constructed from the large Pd_n ($n \geq 4$) cluster decorated graphene are sensitive enough for HCHO detecting with the highest absolute response value over 20% at small bias voltages. Combined with the adsorption energy results we consider that the devices constructed from the Pd_n (n = 5 and 6) cluster decorated graphene should be suitable for HCHO gas sensing. The present work provides a useful guidance for designing the HCHO gas sensors based on small metal cluster decorated graphene.

Conflicts of interest

The authors declare no academic misconducts or competing financial interest.

Acknowledgements

The present study was supported by the National Natural Science Foundation of China (Grant No. 11704041) and GRINM Innovation Foundation fund project.

References

1 K. Kawamura, K. Kerman, M. Fujihara, N. Nagatani, T. Hashiba and E. Tamiya, *Sens. Actuators, B*, 2005, **105**, 495–501.
2 T. Salthammer, S. Mentese and R. Marutzky, *Chem. Rev.*, 2010, **110**, 2536–2572.
3 R. D. Timothy, N. R. Carey, P. Susan, C. D. Glass, B. Geza, R. Alison and F. Lin, *Ann. Occup. Hyg.*, 2015, **60**, 132–138.
4 S. Suresh and T. J. Bandosz, *Carbon*, 2018, **137**, 207–221.
5 J. K. McLaughlin, *Int. Arch. Occup. Environ. Health*, 1994, **66**, 295–301.
6 A. Duong, C. Steinmaus, C. M. McHale, C. P. Vaughan and L. Zhang, *Mutat. Res., Rev. Mutat. Res.*, 2011, **728**, 118–138.
7 Q. Huang, D. Zeng, H. Li and C. Xie, *Nanoscale*, 2012, **4**, 5651–5658.
8 P. R. Chung, C. T. Tzeng, M. T. Ke and C. Y. Lee, *Sensors*, 2013, **13**, 4468–4484.
9 D. Chen and Y. J. Yuan, *IEEE Sens. J.*, 2015, **15**, 6749–6760.
10 I. Cabria, M. J. López, S. Fraile and J. A. Alonso, *J. Phys. Chem. C*, 2012, **116**, 21179–21189.
11 R. Hussain, M. Saeed, M. Y. Mehboob, S. U. Khan, M. Usman Khan, M. Adnan, M. Ahmed, J. Iqbal and K. Ayub, *RSC Adv.*, 2020, **10**, 20595–20607.
12 A. Safavi, N. Maleki, F. Farjami and E. Farjami, *J. Electroanal. Chem.*, 2009, **626**, 75–79.
13 F. Niu and Q. Yi, *Rare Met.*, 2011, **30**, 102–105.
14 H. Yin, H. Tang, D. Wang, Y. Gao and Z. Tang, *ACS Nano.*, 2012, **6**, 8288–8297.
15 D. Sen, R. Thapa and K. K. Chattopadhyay, *Int. J. Hydrog. Energy*, 2013, **38**, 3041–3049.
16 A. Gutés, B. Hsia, A. Sussman, W. Mickelson, A. Zettl, C. Carraro and R. Maboudian, *Nanoscale*, 2012, **4**, 438–440.
17 W. Dong, Y. Ren, Z. Bai, Y. Yang and Q. Chen, *Bioelectrochem*, 2019, **128**, 274–282.
18 R. Kumar, D. Varandani, B. R. Mehta, V. N. Singh, Z. Wen, X. Feng and K. Mullen, *Nanotechnology*, 2011, **22**, 275719.
19 Y. Y. Fan, H. L. Tu, Y. Pang, F. Wei, H. B. Zhao, Y. Yang and T. L. Ren, *Rare Met.*, 2020, **39**, 651–658.
20 Q. Yi, F. Niu and W. Yu, *Thin Solid Films*, 2011, **519**, 3155–3161.

© 2021 The Author(s). Published by the Royal Society of Chemistry

Open Access Article. Published on 18 November 2021. Downloaded on 12/4/2025 3:34:31 PM.
This article is licensed under a Creative Commons Attribution-NonCommercial 3.0 Unported Licence.

21 K. Czelej, K. Cwieka, J. C. Colmenares and K. J. Kurzydlowski, *Langmuir*, 2016, **32**, 7493–7502.
22 M. Yoosefian, H. Raissi and A. Mola, *Sens. Actuators, B*, 2015, **212**, 55–62.
23 J. Deng, W. Song, M. Jing, T. Yu, Z. Zhao, C. Xu and J. Liu, *Catal. Today*, 2020, **339**, 210–219.
24 L. Yang, W. Xiao, J. Wang, X. Li and L. Wang, *J. Mater. Sci.*, 2021, **56**, 12256–12269.
25 G. Kresse and J. Furthmüller, *Comput. Mater. Sci.*, 1996, **6**, 15–50.
26 G. Kresse and J. Furthmüller, *Phys. Rev. B: Condens. Matter Mater. Phys.*, 1996, **54**, 11169.
27 J. P. Perdew, K. Burke and M. Ernzerhof, *Phys. Rev. Lett.*, 1996, **77**, 3865.
28 G. Kresse and D. Joubert, *Phys. Rev. B: Condens. Matter Mater. Phys.*, 1999, **59**, 1758–1775.
29 S. Grimme, *J. Comput. Chem.*, 2006, **27**, 1787–1799.
30 J. Zhou, Q. Wang, Q. Sun, X. Chen, Y. Kawazoe and P. Jena, *Nano Lett.*, 2009, **9**, 3867–3870.
31 G. Henkelman, A. Arnaldsson and H. Jónsson, *Comput. Mater. Sci.*, 2006, **36**, 354–360.
32 W. Tang, E. Sanville and G. Henkelman, *J. Phys.: Condens. Matter*, 2009, **21**, 084204.
33 J. Taylor, H. Guo and J. Wang, *Phys. Rev. B: Condens. Matter Mater. Phys.*, 2001, **63**, 245407.
34 D. Waldron, P. Haney, B. Larade, A. MacDonald and H. Guo, *Phys. Rev. Lett.*, 2006, **96**, 166804.
35 M. Brandbyge, N. Kobayashi and M. Tsukada, *Phys. Rev. B: Condens. Matter Mater. Phys.*, 1999, **60**, 17064–17070.
36 M. Brandbyge, J. L. Mozos, P. Ordejón, J. Taylor and K. Stokbro, *Phys. Rev. B: Condens. Matter Mater. Phys.*, 2002, **65**, 165401.
37 S. Datta, *Quantum transport: atom to transistor*, Cambridge University Press, 2005.
38 M. Büttiker, Y. Imry, R. Landauer and S. Pinhas, *Phys. Rev. B: Condens. Matter Mater. Phys.*, 1985, **31**, 6207–6215.
39 J. Rogan, G. García, J. A. Valdivia, W. Orellana, A. H. Romero, R. Ramírez and M. Kiwi, *Phys. Rev. B: Condens. Matter Mater. Phys.*, 2005, **72**, 115421.
40 J. A. Alonso, *Structure and properties of atomic nanoclusters*, Imperial College Press, London, 2005.
41 I. Cabria, M. J. López and J. A. Alonso, *Phys. Rev. B: Condens. Matter Mater. Phys.*, 2010, **81**, 035403.
42 W. Xiao, R. Zeng, L. Cheng, J. W. Wang, L. J. Jiang and L. G. Wang, *RSC Adv.*, 2015, **5**, 61861–61867.
43 E. Jeroro and J. M. Vohs, *J. Am. Chem. Soc.*, 2008, **130**, 10199–10207.
44 X. K. Gu and W. X. Li, *J. Phys. Chem. C*, 2010, **114**, 21539–21547.
45 X. Chen, L. Xu, L. L. Liu, L. S. Zhao, C. P. Chen, Y. Zhang and X. C. Wang, *Appl. Surf. Sci.*, 2017, **396**, 1020–1025.
46 M. Zhou, Y. H. Lu, Y. Q. Cai, C. Zhang and Y. P. Feng, *Nanotechnology*, 2011, **22**, 385502.
47 D. B. Farmer, R. Golizadeh Mojarad, V. Perebeinos, Y. M. Lin, G. S. Tulevski, J. C. Tsang and P. Avouris, *Nano Lett.*, 2009, **9**, 388–392.
48 L. Kou, T. Frauenheim and C. Chen, *J. Phys. Chem. Lett.*, 2014, **5**, 2675–2681.
49 K. Lee, R. Gatensby, N. McEvoy, T. Hallam and G. S. Duesberg, *Adv. Mater.*, 2013, **25**, 6699–6702.
50 S. Yang, C. Jiang and S. h. Wei, *Appl. Phys. Rev.*, 2017, **4**, 021304.
51 A. J. Yang, D. W. Wang, X. H. Wang, J. F. Chu, P. L. Lv, Y. Liu and M. Z. Rong, *IEEE Electron Device Lett.*, 2017, **38**, 963–966.
52 S. J. Young and Z. D. Lin, *ECS J. Solid State Sci. Technol.*, 2017, **6**, M130–M132.
53 F. Niu, L. M. Tao, Y. C. Deng, Q. H. Wang and W. G. Song, *New J. Chem.*, 2014, **38**, 2269–2272.

© 2021 The Author(s). Published by the Royal Society of Chemistry